Mother Wavelet Performance Evaluation for Noise Removal in Partial Discharge Signals

Isara Sornsen[1], **Chatchai Suppitaksakul**[1†], and **Pollakrit Toonkum**[2], Non-members

ABSTRACT

This article aims to study the pattern of partial discharge (PD) signals occurring on the insulators of high-voltage systems. A mother wavelet comparison and wavelet decomposition are presented to detect and locate PD signals by dividing them into three processes: 1) signal test generation, employing RC and RLC impedance circuits whereby the output voltage pulses in the RC impedance circuit are expressed as damped exponential pulses (DEPs) and those of the RLC as damped oscillatory pulses (DOPs). White Gaussian noise (AWGN) is then added, which mimics the effect of many random processes in measurement systems. The concept involves applying noise to the original signal and removing it with wavelet transform using various wavelet templates such as Daubechies, Coiflet, Symlet, and biorthogonal to separate the signal components. The experiment results are then compared, and a performance evaluation performed using mean square error (MSE) as in the first two signals. 2) DEPs and DOPs are added with a sine wave to simulate a virtual measurement from a measuring instrument according to the superposition principle using a band-pass filter with the frequency range specified by the two elements to determine the frequency of the resulting PD. 3) The results of the PD signal experiments developed in the laboratory are also evaluated for efficiency by subjective measurement by a PD signal specialist. Therefore, partial discharge denoising is evaluated using the mother wavelet as a preprocessing step for feature extraction and classification.

Keywords: Partial Discharge, Wavelet Transform, WT, Mean Square Error, MSE, Subjective Measurement

1. INTRODUCTION

The reliability of equipment affects the stability of an electrical system. To maintain reliability, regular electrical checks are required. Most failures in high-voltage systems are caused by the failure of insulating components as summarized in Table 1. In general, the dielectric properties of insulating materials can deteriorate due to factors such as heat, chemical interaction, current, or the connection of system components. According to diagnostic research on insulating materials [1], in most cases, electrical faults directly result from partial discharge (PD), which is a leading cause of corrosion and deterioration in the insulation system. Without preventive maintenance, it will eventually cause electrical equipment failure, leading to safety, environmental, and economic problems in the production process. Therefore, it is necessary to diagnose high-voltage equipment problems to determine and predict current and future conditions and prolong the remaining service life [2].

***Table 1**: Contributors to system failure and failure due to insulation problems in high-voltage equipment [1].*

Equipment	Contribution to System Failure (%)	Failure due to Insulation Problems (%)
Insulators	35	90
Generators	15	47
Transformers	12	84
GIS and switchgear	15	95
Power cables	10	89

PD occurs in many devices, including switchgear, transformers, cables or transmission lines, underground cables, and generators. Several methods can be employed to measure PD, the most common being the use of sensors (coupling devices), detectors, and instrumentation of the test object (Fig. 1). Methods for PD pattern recognition have also been developed over the years, such as statistical analysis, neural networks, fuzzy logic, wavelet transformation, fractal analysis, and time-frequency clustering [3].

The partial discharge signal has a high frequency of around 50–250 MHz, and noise occurs in the frequency range of 5–49 MHz, as shown in Fig. 2, with a pulse width of at least 1–5 ns rise time from the signal frequency. The PD will be in 1/(4 × rise time), as shown in Fig. 3.

2. SIGNAL ANALYSIS WITH WAVELET TRANSFORM

The Fourier transform (FT) is a mathematical signal analysis tool in the frequency domain. In signal processing, the FT is widely used since it can describe complex

Manuscript received on February 2, 2022; revised on May 27, 2022; accepted on June 7, 2022. This paper was recommended by Associate Editor Kriangkrai Sooksood.

[1]The authors are with the Department of Electrical Engineering, Rajamangala University of Technology Thanyaburi, Pathum Thani, Thailand.

[2]The author is with the College of Integrated Science and Technology, Rajamangala University of Technology Lanna, Chiangmai, Thailand.

[†]Corresponding author: chatchai.s@en.rmutt.ac.th

Digital Object Identifier: 10.37936/ecti-eec.2022203.247521

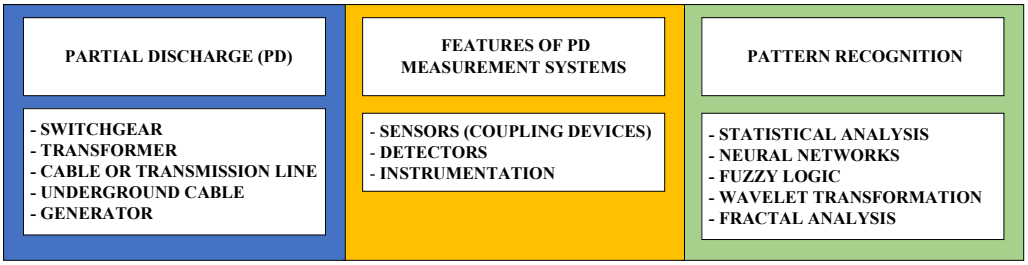

***Fig. 1**: PD measurement technologies specifically developed to improve PD diagnostic methods [3–6].*

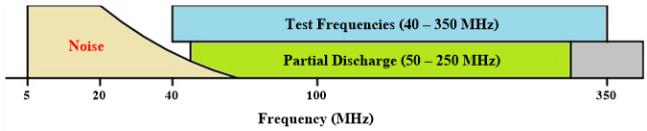

***Fig. 2**: Frequency of the PD signal [7].*

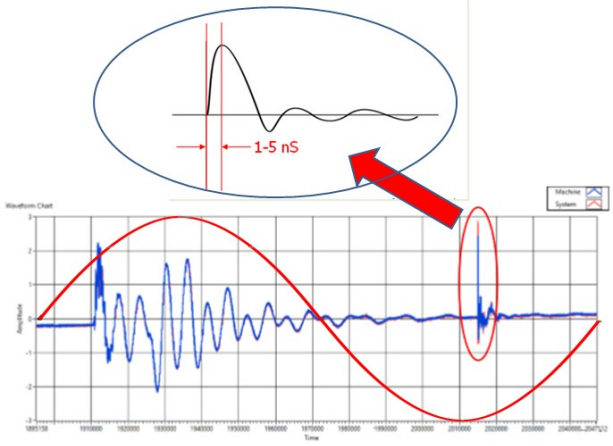

***Fig. 3**: Characteristics of the PD signal [3].*

signals in sine and cosine elements which are significant because they form the basis for considering other signals. The signals can be easily converted from the time domain to the frequency domain using FT, which describes the signals in spectrum form. Also, it can be considered a fundamental signal analysis in the form of an exponential function. However, a limitation of the FT is that in non-stationary signal change analysis, the errors will occur, including missing timing data.

The FT employs constant signal analysis intervals to analyze signals of all frequencies. Consequently, it is unsuitable in practice since the partial discharging signals are high frequency and change rapidly. Thus, it is better to use narrow intervals for the analysis of high-frequency signals.

Since the low frequency changes slowly, a wider interval should be used for analysis, and the FT has been developed for this reason. A signal analysis format with an analytical resolution adjustment called wavelet transform (WT) describes the structure of a signal. It consists of a specific group of signals combined into one specific signal and is a constantly changing wave which changes in size, rapidly reducing to zero on both sides. Wavelet transform combines multiple wavelets to describe the structure of any signal where each wavelet is structured from the same function. This function is a wavelet origin called a mother wavelet. Each wavelet is contained within this wavelet set, where each wave is formed by scaling a and a translation b. Therefore, if $\psi(t)$ is the mother, wavelets can be described by Eq. (1).

$$\psi_{b,a}(t) = \frac{1}{\sqrt{a}}\psi\left(\frac{t-b}{a}\right) \tag{1}$$

The wavelet function in time t is scaled and moved by parameters a and b, respectively, where the conversion interval and frequency are relative. In order for the scaled wavelet to have the same energy as the parent wavelet, it always needs to be normalized by $1/\sqrt{a}$.

Wavelet theory is used to describe the decomposition of components decomposed into relatively smaller parts which take the form of scaled and translated wavelets. Thus, it refers to any signal that can be generated using a basic function. Wavelet decomposition is a wavelet transform in itself. Likewise, wavelet reconstruction is an inverse wavelet transform (IWT) which brings together these sub-components to form the original signal.

2.1 Daubechies Wavelet

Ingrid Daubechies, one of the world's most prominent wavelet researchers, has discovered what is known as a "compactly-supported orthonormal wavelet." It was created to analyze discrete wavelets in practice. The Daubechies wavelet is generally abbreviated into Db, and for the order N is written as DbN [8].

2.2 Coiflet Wavelet

Daubechies created this type of wavelet to satisfy the requirements of R. Coifman. The Coiflet wavelet is a basic function, almost asymmetric in nature. The Coiflet wavelet can be abbreviated into Coif and for the order N is written as CoifN [8].

2.3 Symlet Wavelet

The symlet wavelet is almost symmetrical. It has been updated from the Daubechies wavelet. The properties of these two wavelets are similar. Symlet wavelet can be

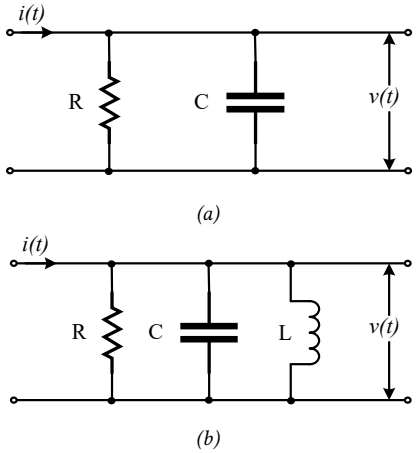

***Fig. 4**: The impedance circuit; (a) RC and (b) RLC.*

abbreviated into Sym, and for the order N is written as SymN [8].

2.4 Biorthogonal Wavelet

The biorthogonal wavelet represents the linear phase properties used to restore the signal and image. It consists of two wavelets, one for factoring and the other for rebuilding to replace it with another identical one. The biorthogonal wavelet can be abbreviated into Bior, and for the order N is written as BiorN.

3. PERFORMANCE EVALUATION AND DISCUSSION

3.1 Damped Exponential Pulses and Damped Oscillatory Pulses

Partial discharge signals need to be generated for use as test signals. Test signal generation employs ***RC*** and ***RLC*** impedance circuits, where the output voltage pulses in the ***RC*** impedance circuit are expressed as damped exponential pulses (DEPs), and the output voltage pulses of the ***RLC*** impedance circuit expressed as damped oscillatory pulses (DOPs) are shown in Fig. 4(a) and 4(b), respectively. The mathematical functions used to generate the DEP and DOP signals are performed according to Eqs. (2) and (3), respectively.

$$\mathrm{DEP}(t) = A\left(e^{-\frac{(t-t_0)}{t_1}} - e^{-\frac{(t-t_0)}{t_2}}\right) \tag{2}$$

$$\mathrm{DOP}(t) = A\sin\left(2\pi f_c\left(t-t_0\right)\right)\left(e^{-\frac{(t-t_0)}{t_1}} - e^{-\frac{(t-t_0)}{t_2}}\right) \tag{3}$$

where A is the maximum pulse signal, t_1 and t_2 are the damping coefficients, t_0 is the time of occurrence, and f_c is the oscillation frequency of the DOP. Values of A and f_c are set at 5 mV and 500 kHz with a sampling rate of 10 MHz. The test signals are generated according to the

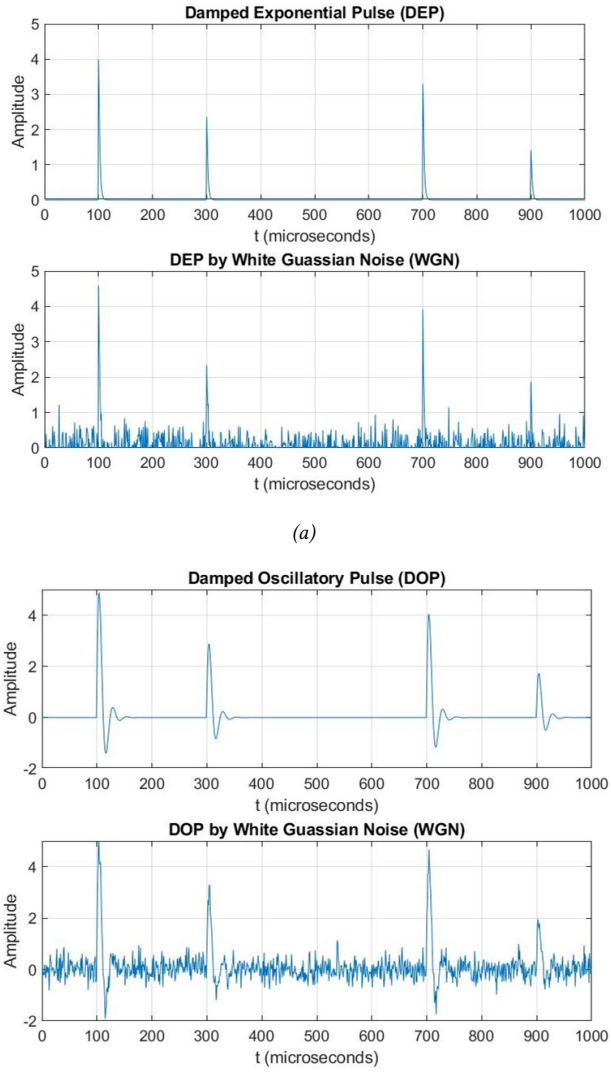

***Fig. 5**: (a) DEP signals and DEP signals with WGN, (b) DOP signals and DOP signals with WGN.*

DEPs (Eq. (2)) and DOPs (Eq. (3)). White Gaussian noise (WGN) is added to both signals (Eq. (4)), which mimic the effect of many random processes in measurement systems, where Y_i are input signals, X_i are output signals and Z_i are noise signals of 10 dBW, generated using the MATLAB program as shown in Fig. 5(a) and 5(b).

$$Y_i = X_i + Z_i \tag{4}$$

The generated PD signals will be taken into WT as a filter to remove noise. Various wavelet templates are employed: Daubechies, Coiflet, symlet, and biorthogonal to act as noise removers by separating the components of the PD signals. Then the results of each wavelet template will be compared, and the PD signals without noise and filtered signals are evaluated by mean square error (MSE) Eq. (5) [9–13].

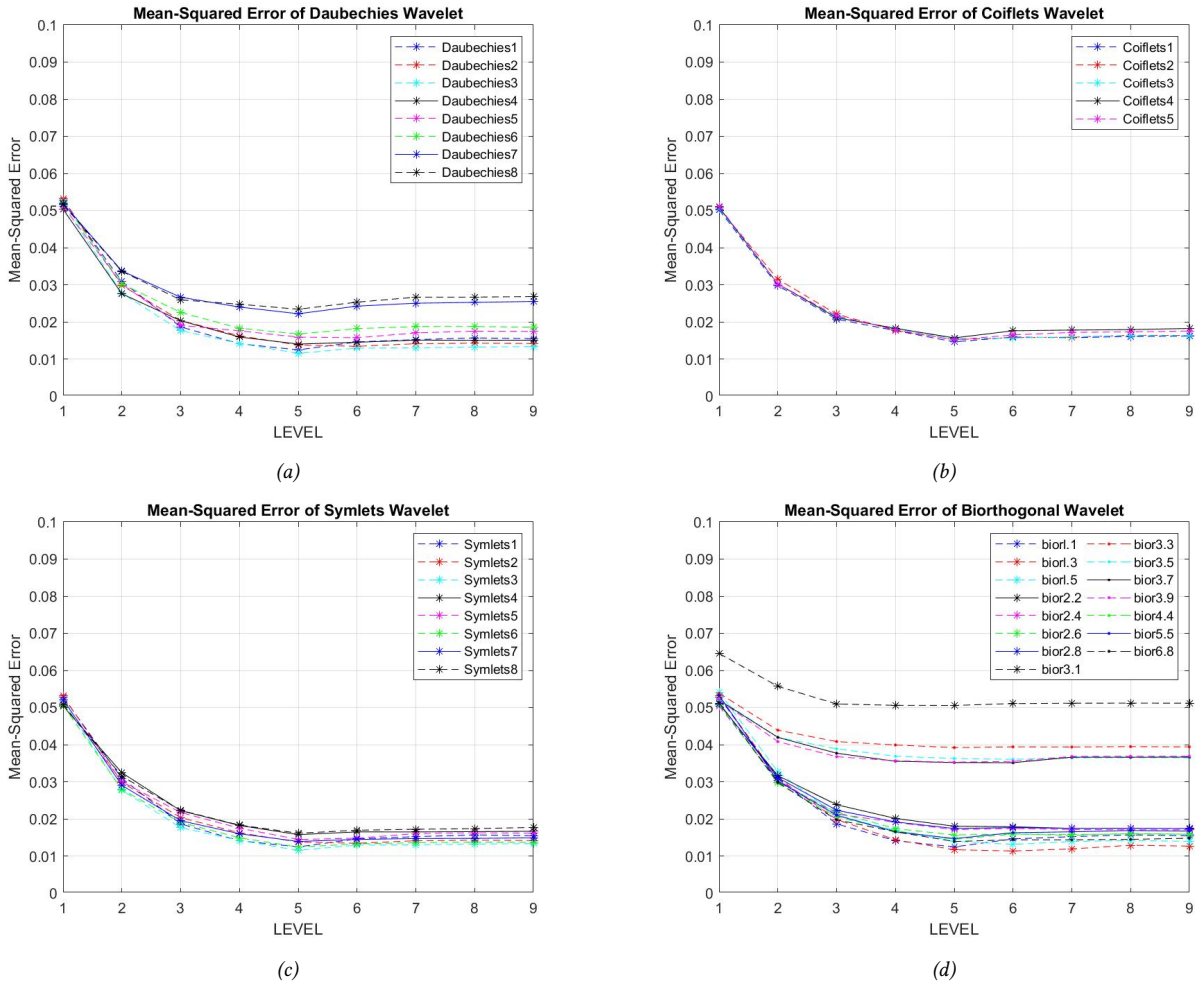

***Fig. 6**: The WT performance results for the DEP signals; (a) Daubechies wavelet, (b) Coiflet wavelet, (c) symlet wavelet, and (d) biorthogonal wavelet.*

***Table 2**: Denoising comparison performed on the DEP signals using four different types of mother wavelets.*

Mother Wavelet	Level	Mean Square Error (MSE)
Db3	5	0.0115
Coif1	5	0.0146
Sym3	5	0.0115
Bior1.3	6	0.0113

***Table 3**: Denoising comparison performed on the DOP signals using four different types of mother wavelets.*

Mother Wavelet	Level	Mean Square Error (MSE)
Db4	9	0.0128
Coif2	6	0.0131
Sym8	5	0.0138
Bior6.8	6	0.0160

$$\mathrm{MSE} = \frac{1}{N}\sum_{i=1}^{N}(F(i) - R(i))^2 \tag{5}$$

where N is the length of the PD signals, F is the PD signal without noise, and R the filtered PD signals.

In Fig. 6, the biorthogonal wavelet (Bior1.3 with level 6) provides the lowest MSE value of the DEP signal at about 0.0113. As can be observed from Fig. 7, the Daubechies wavelet (Db4 level 9) gave the lowest MSE value for the DOP signal, at 0.0128. All WT performance results for the DEP and DOP signals are listed in Tables 2 and 3, respectively. The DEP and DOP signals without noise are plotted for comparison with the filtered signals passing through the noise-removing process, as shown in Figs. 8 and 9.

3.2 Partial Discharge Signal Generation

According to the concept of PD data acquisition into the computer memory [14], the natural form of discharge is based on a sinusoidal waveform at the actual operating voltage with a frequency of 50 Hz [15]. It takes place as

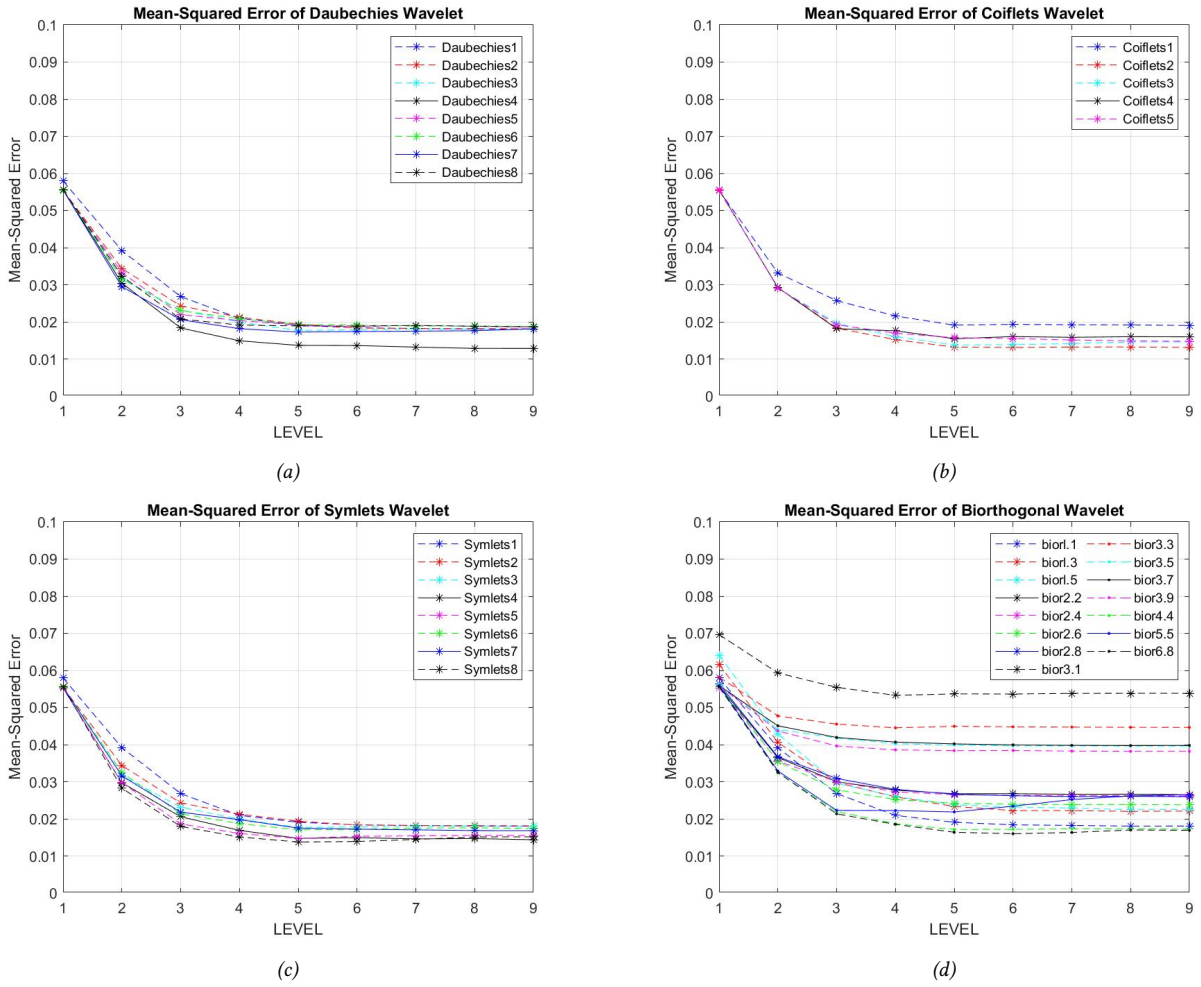

***Fig. 7**: The WT performance results for the DOP signals; (a) Daubechies wavelet, (b) Coiflet wavelet, (c) symlet wavelet, and (d) biorthogonal wavelet.*

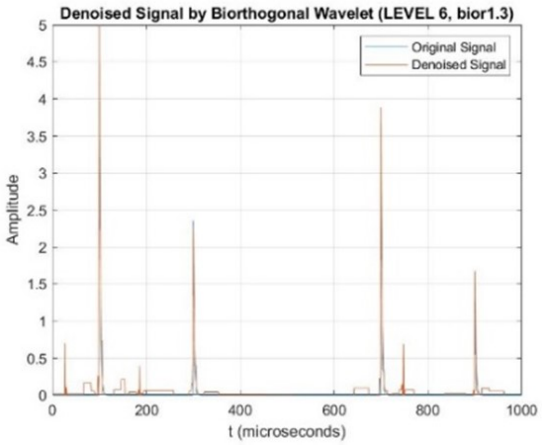

***Fig. 8**: Noise removal of the DEP signals with level 6 Bior1.3.*

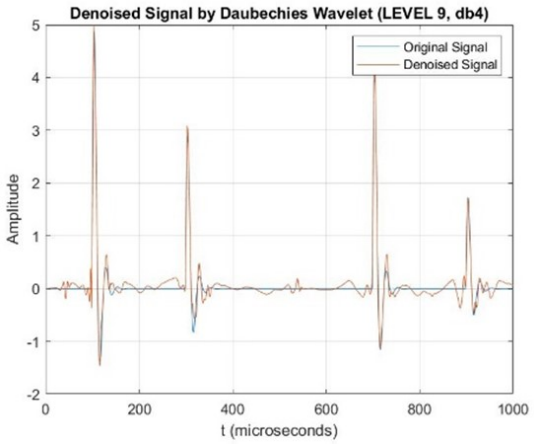

***Fig. 9**: Noise removal of the DOP signals with level 9 Db4.*

two pulses when discharge pulses occur in the positive and negative cycles resulting from the discharge of the latent capacitance within the insulator compared to the actual working pressure. The DEP ($y(t)$) and DOP ($z(t)$) are superimposed on a fundamental sine wave to simulate a virtual measurement from the measuring instrument where A is the maximum pulse signal, f is 50 Hz, f_c is set as a constant [16] 58 MHz with a sampling rate of 300 MHz, and t the time of occurrence. The mathematical functions used to generate $y(t)$ and $z(t)$

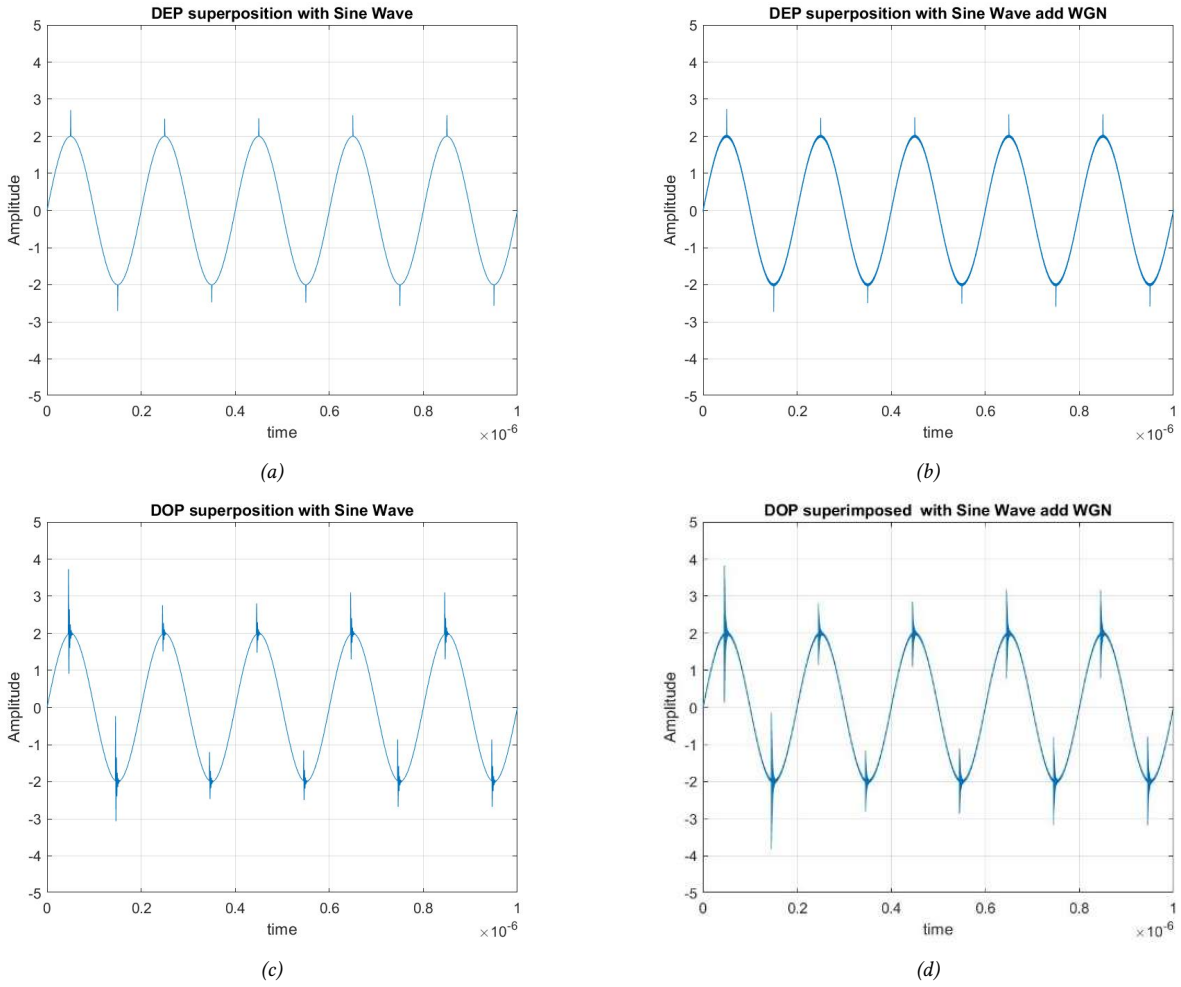

***Fig. 10**: (a) DEP superimposed with a sine wave, (b) DEP superimposed with a WGN added to the sine wave, (c) DOP superposition with a sine wave, and (d) DOP superimposed with a WGN added to the sine wave.*

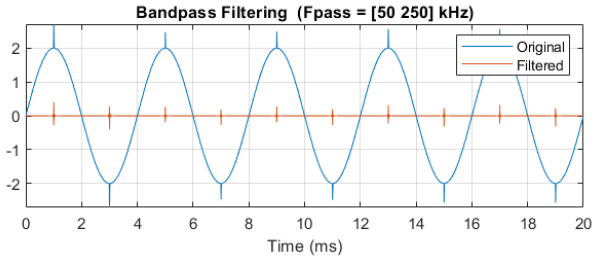

***Fig. 11**: DEP signal using a band-pass filter with a passband frequency range of 50–250 MHz.*

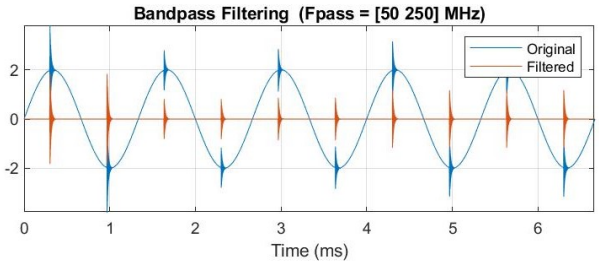

***Fig. 12**: DOP signal using a band-pass filter with a passband frequency range of 50–250 MHz.*

are performed according to Eqs. (6) and (7) with white Gaussian noise (WGN) added at 40 dBW. Therefore, the PD signals can be generated shown in Fig. 10.

$$y(t) = A\sin(2\pi f t) + \mathrm{DEP}(t) \tag{6}$$

$$z(t) = A\sin(2\pi f t) + \mathrm{DOP}(t) \tag{7}$$

The DEP and DOP superimposed signals in Figs. 10(a) and 10(c) are filtered using a band-pass filter with the passband frequency range specified by the two elements (around 50–250 MHz). At the band-pass filter, the low-frequency signal (50 Hz) is removed. The original and filtered signals and their spectra are plotted as shown in Figs. 11 and 12. Fast Fourier transform (FFT) is employed to convert the signal from the time domain to the frequency domain to determine the frequency of the PD. The results reveal that the frequency of the signal in Fig. 11 is 76 MHz, and frequency of the signal in Fig. 12

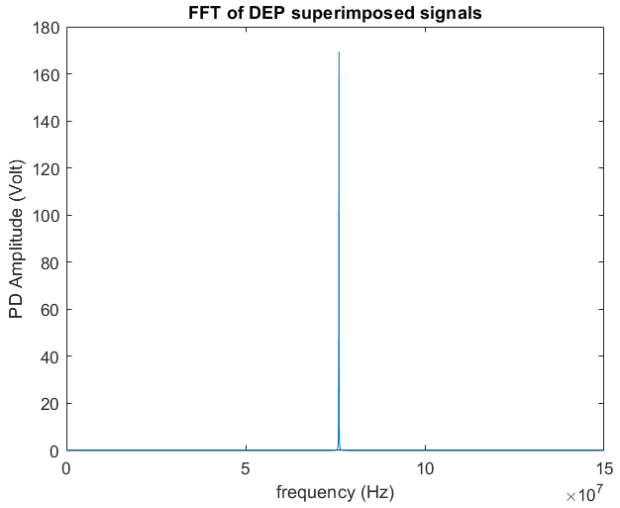

Fig. 13: FFT of the DEP superimposed signal.

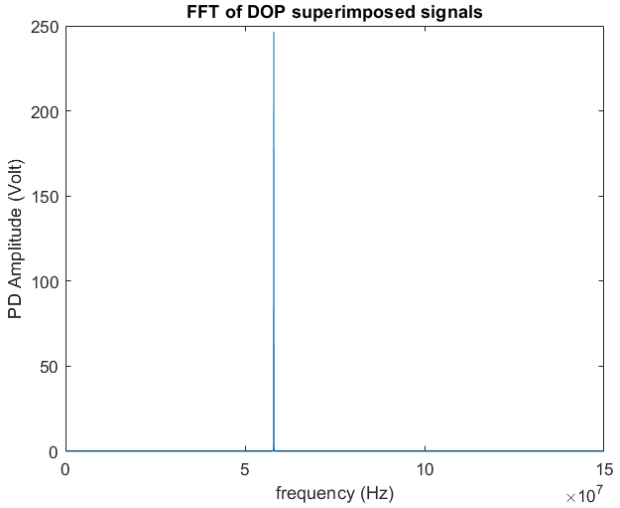

Fig. 14: FFT of the DOP superimposed signal.

is 58 MHz, as shown in Figs. 13 and 14, respectively. Based on the above method, the idea is to determine the frequency of a PD signal as noise or PD signals to analyze the input signal by passing a band-pass filter in the signal frequency band to determine the PD signals, then use FFT to determine the frequency of the resulting PD signals. If the incoming input signal is not in the frequency range of the PD signal, it can be referred to as noise [17].

3.3 PD Signals of Experiments Developed in the Laboratory

The connection of the PD measuring system in the test circuit is different from that in the impedance connection (Z_m), which is the standard for measuring PD according to IEC 60270 [18, 19]. Known as a coupling device (CD), it assembles the measurement impedance (Z_{mi}) at the beginning of the system, as shown in Fig. 15. Fig. 15 shows a straight PD detection circuit where U~ is a high-voltage supply, Z_{mi} the input impedance of the measuring system, CC is the connecting cable, C_a a test object, C_k a coupling capacitor, CD a coupling device, MI the measuring instrument, and Z is a filter. The filter prevents high-frequency interference from the high-voltage supply to the test circuit. At the same time, it acts to prevent PD from escaping from the test material through the high-voltage supply. This filter can consist of either L or C and PD signals from experiments developed in the laboratory for changing electrical insulators (pin insulators) rather than C_a, as shown in Fig. 16.

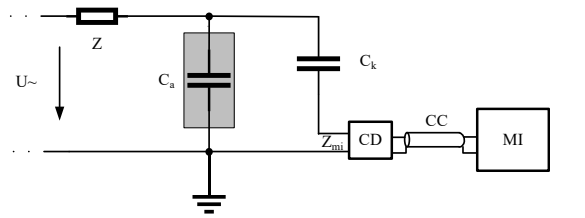

Fig. 15: Measuring PD according to the IEC 60270 standard.

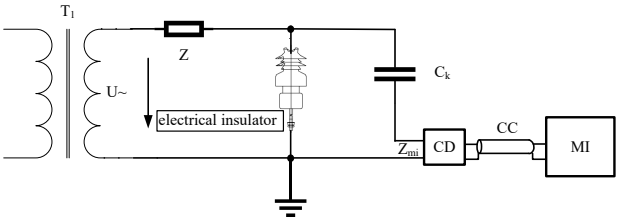

Fig. 16: Electrical insulator instead of C_a.

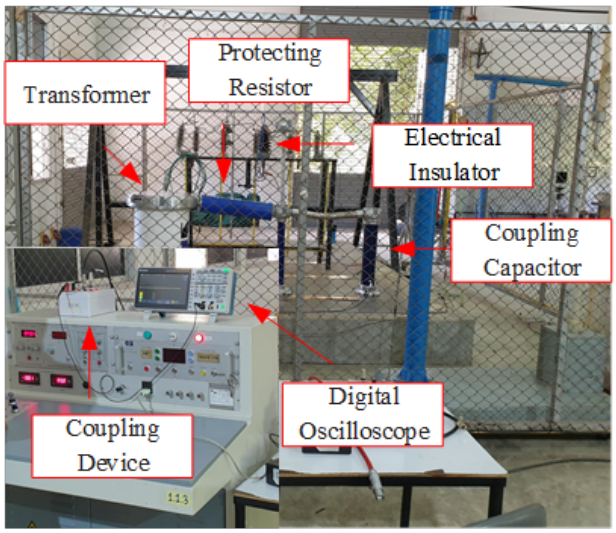

Fig. 17: Experimental setup performed in the laboratory.

3.3.1 Experimental setup

Fig. 17 shows the experimental setup. A single-phase high-voltage 100 kV transformer was set up, labeled T_1. A protecting resistor Z (10 MΩ) was employed to protect the transformer against overcurrent in the case of flashover on the test object, along with a 22 kV electrical insulator (pin). The coupling capacitor (100 pF) was used to transfer the PD current signals to the coupling device, with a connection cable (CC) to the

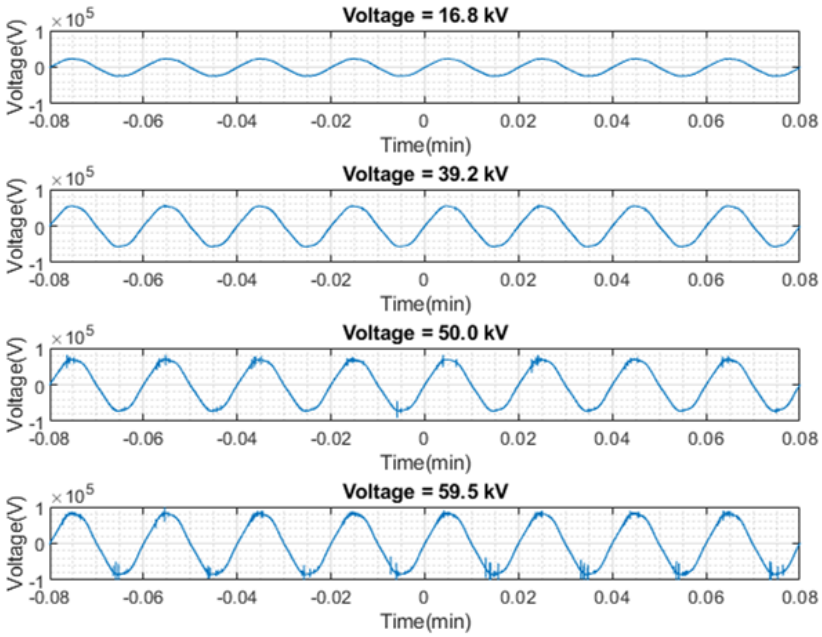

***Fig. 18**: Adjusting the voltage increase until the breakdown of the insulator.*

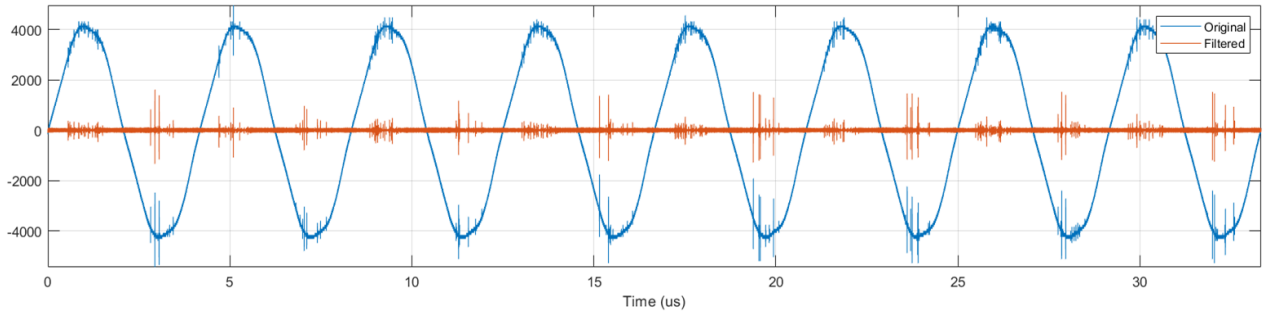

***Fig. 19**: PD signals on the electrical insulator using a band-pass filter with a specified frequency range of around 50–250 MHz.*

measuring instrument (MI). A coupling device translates these current signals to the voltage signals, measurable by the digital oscilloscope. The digital oscilloscope is a Tektronix TBS 2000B, selected based on the sampling rate (2 GS/s maximum), display, weight and dimensions, ease and flexibility of use, and cost. An oscilloscope is a digital data acquisition device that translates the analog PD signals into digital samples. In this experiment, a sampling rate of 500 MHz is applied.

3.3.2 Measurements and results

The insulator PD signals mentioned above were measured to observe the insulator PD waveform, starting from low voltage input and then gradually increasing the voltage.

The voltage is increased until the breakdown of the insulator, as shown in Fig. 18. When adjusting the higher voltage, the PD signal is measured by the insulator. Since the increased voltage causes an insulator breakdown, the dielectric strength is reduced, causing a flashover phenomenon on the surface insulator.

The next step is to take a band-pass filter with a frequency range of 50–250 MHz to analyze the input signal, either a PD or noise signal. Fig. 19 shows the nature of the PD signals occurring on the insulator when filtered with a band-pass filter. A passband frequency range of 50–250 MHz was used to observe the shape of the PD signal prior to the insulation breakdown.

The next step is to use the fast Fourier transform (FFT) to convert the signal from the time domain to the frequency domain to determine the frequency of the resulting PD. The signal frequencies shown in Fig. 20 are 50 Hz and 142 MHz, respectively, as can be seen by FFT of the signal in Fig. 21. Two frequencies can be observed: 50 Hz for the sinusoidal waveform and 142 MHz for the PD signals. From Fig. 20, the noise resulting from the measurement circuit on the surrounding environment [20] will be removed by WT using the Daubechies, Coiflet, symlet, and biorthogonal wavelet templates to separate the components of the signal and evaluate them for efficacy using the PD signal specialist's subjective measurements, respectively, as shown in Fig. 22.

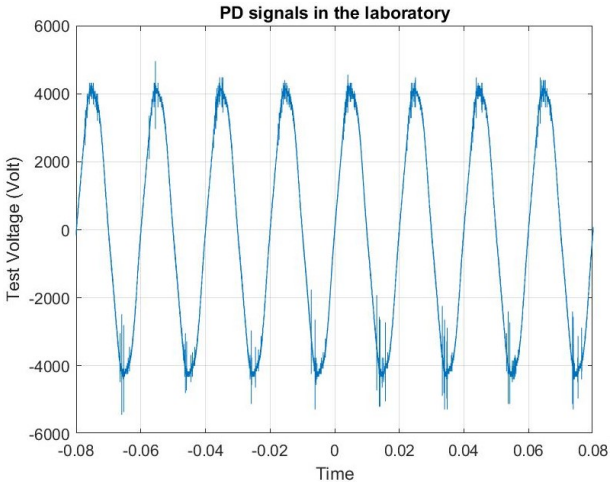

Fig. 20: *PD signals of experiments developed in the laboratory.*

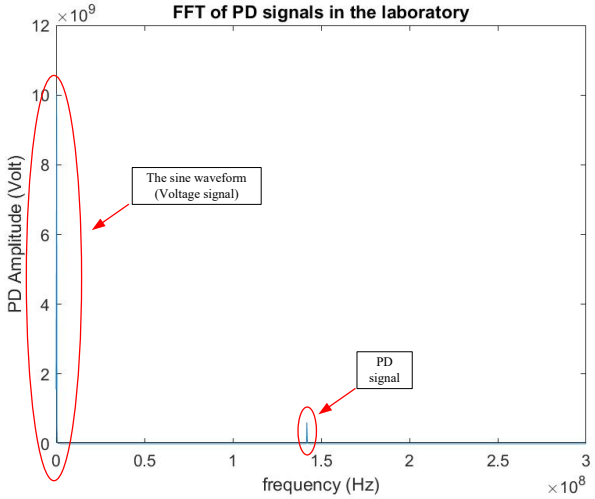

Fig. 21: *FFT of PD signals from experiments developed in the laboratory at 50 Hz and 142 MHz.*

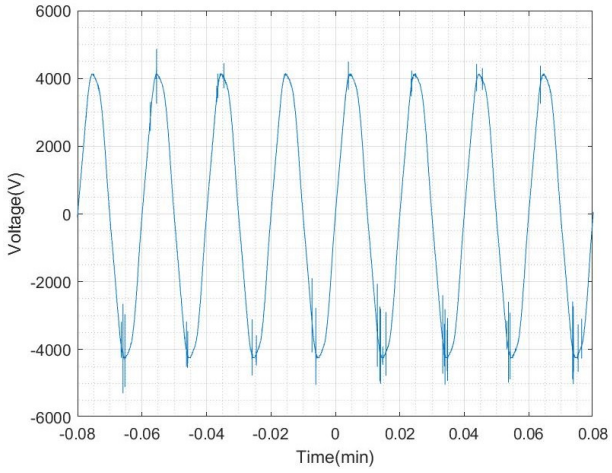

(a) Db7

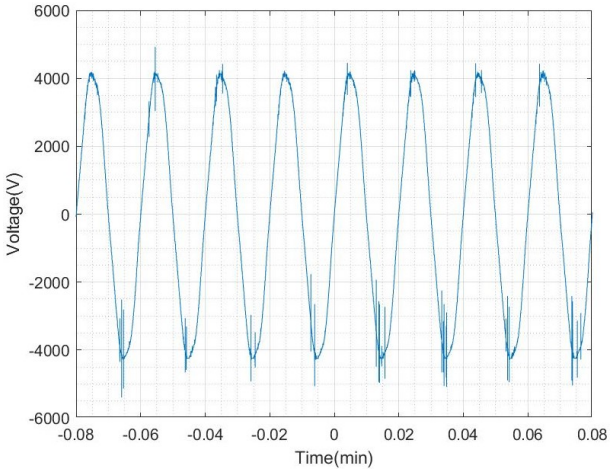

(b) Coif5

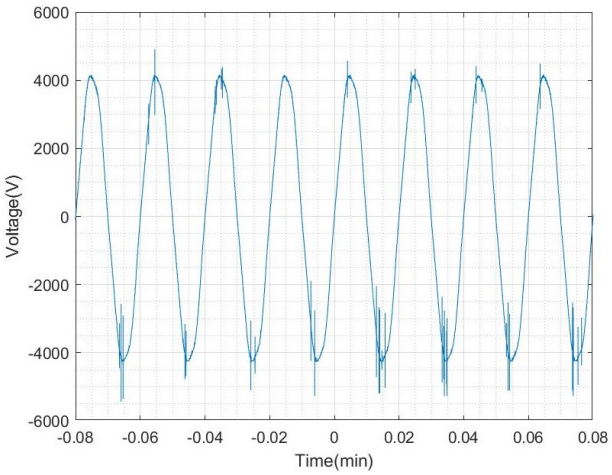

(c) Sym5

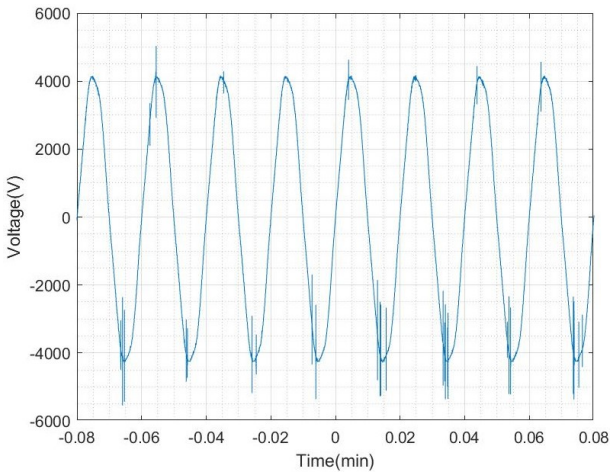

(d) Bior3.5

Fig. 22: *The results of the experiment are compared and the performance evaluated by the subjective measurement of PD signals; (a) Db7, (b) Coif5, (c) Sym5, and (d) Bior3.5.*

As can be observed from Fig. 22, the PD signal specialist's subjective measurements were Db7, Coif5, Sym5, and Bior3.5. It can reduce noise effectively and retain the shape of the PD signals. When comparing the four types of mother wavelets, Sym5 is most suitable for the attenuation of PD waveforms obtained in laboratory testing.

4. CONCLUSION

From the results presented in this paper, it can be concluded that the processing technique for detecting PD signals to determine the frequency of the resulting PD signal can be achieved using a band-pass filter when the PD signal is obtained. The frequency band of the PD signal is then attenuated using different mother wavelets to determine the appropriateness of the noise reduction, completing the shape of the PD signal. Such information can be used to develop a process for classifying the pattern of the PD signals. The various PD signals can be further used in the diagnosis and troubleshooting of partial discharge signals.

ACKNOWLEDGMENTS

The authors wish to thank the High Voltage Research Laboratory (HVRL), Department of Electrical Engineering Rajamangala University of Technology Lanna, Chiangrai, Thailand, for providing the data used in Section 3.3 of the paper.

REFERENCES

[1] Suwarno, "Partial discharges in high voltage insulations: Mechanism, patterns and diagnosis," in *2014 International Conference on Electrical Engineering and Computer Science (ICEECS)*, 2014, pp. 369–375.

[2] W. J. K. Raymond, L. T. Sing, L. W. Kin, G. K. Meng, H. A. Illias, and A. H. A. Bakar, "Feature pruning for partial discharge classification using IndFeat and ReliefF algorithm," in *2018 IEEE 2nd International Conference on Dielectrics (ICD)*, 2018.

[3] G. Stone, "Partial discharge diagnostics and electrical equipment insulation condition assessment," *IEEE Transactions on Dielectrics and Electrical Insulation*, vol. 12, no. 5, pp. 891–903, Oct. 2005.

[4] Y. Luo, Z. Li, and H. Wang, "A review of online partial discharge measurement of large generators," *Energies*, vol. 10, no. 11, 2017, Art. no. 1694.

[5] J. Fuhr and T. Aschwanden, "Identification and localization of PD-sources in power-transformers and power-generators," *IEEE Transactions on Dielectrics and Electrical Insulation*, vol. 24, no. 1, pp. 17–30, Feb. 2017.

[6] W. J. K. Raymond, H. A. Illias, A. H. A. Bakar, and H. Mokhlis, "Partial discharge classifications: Review of recent progress," *Measurement*, vol. 68, pp. 164–181, May 2015.

[7] IRIS Power, "Module 1: Basic PD theory, detection and characteristics."

[8] A. Zaeni, T. Kasnalestari, and U. Khayam, "Application of wavelet transformation symlet type and coiflet type for partial discharge signals denoising," in *2018 5th International Conference on Electric Vehicular Technology (ICEVT)*, 2018, pp. 78–82.

[9] A. A. Soltani and S. M. Shahrtash, "Decision tree-based method for optimum decomposition level determination in wavelet transform for noise reduction of partial discharge signals," *IET Science, Measurement & Technology*, vol. 14, no. 1, pp. 9–16, Jan. 2020.

[10] C. F. Cunha, A. T. Carvalho, M. R. Petraglia, H. P. Amorim, and A. C. Lima, "Proposal of a novel fitness function for evaluation of wavelet shrinkage parameters on partial discharge denoising," *IET Science, Measurement & Technology*, vol. 12, no. 2, pp. 283–289, Mar. 2018.

[11] S. H. K. Hamadi, M. Isa, L. M. Ishak, M. N. K. H. Rohani, C. C. Yii, B. Ismail, and M. Shafiq, "Evaluation of denoising performance indices for noisy partial discharge signal based on DWT technique," in *2017 IEEE 15th Student Conference on Research and Development (SCOReD)*, 2017, pp. 392–397.

[12] D. Evagorou, A. Kyprianou, P. L. Lewin, A. Stavrou, V. Efthymiou, and G. E. Georghiou, "Evaluation of partial discharge denoising using the wavelet packets transform as a preprocessing step for classification," in *2008 Annual Report Conference on Electrical Insulation and Dielectric Phenomena*, 2008, pp. 387–390.

[13] B. Raghavendra and M. K. Chaitanya, "Comparative analysis and optimal wavelet selection of partial discharge de-noising methods in gas-insulated substation," in *2017 Third International Conference on Advances in Electrical, Electronics, Information, Communication and Bio-Informatics (AEEICB)*, 2017.

[14] M. Hikita, K. Yamada, A. Nakamura, T. Mizutani, A. Oohasi, and M. Ieda, "Measurements of partial discharges by computer and analysis of partial discharge distribution by the monte carlo method," *IEEE Transactions on Electrical Insulation*, vol. 25, no. 3, pp. 453–468, Jun. 1990.

[15] Y. Zhou, Y. Qin, and C. Leach, "Cost-effective online partial discharge measurements for electrical machines: Preventing insulation failure," *IEEE Electrical Insulation Magazine*, vol. 26, no. 5, pp. 23–29, Sep. 2010.

[16] J. Wu, A. R. Mor, P. V. van Nes, and J. J. Smit, "Measuring method for partial discharges in a high voltage cable system subjected to impulse and superimposed voltage under laboratory conditions," *International Journal of Electrical Power & Energy Systems*, vol. 115, Feb. 2020, Art. no. 105489.

[17] P. Jitjing, C. Suppitaksakul, and W. Boonphen, "Partial discharge signals detecting and preventive maintenance planning for 21 kV generator case study of a generator at the combined cycle power plant of Ratchaburi power company limited," in

2018 15th International Conference on Electrical Engineering/Electronics, Computer, Telecommunications and Information Technology (ECTI-CON), 2018, pp. 41–44.

[18] *High-voltage test techniques - Partial discharge measurements*, IEC 60270, International Electrotechnical Commission, Geneva, Switzerland, 2000.

[19] B. Liu, H. Ma, and P. Ju, "Partial discharge diagnosis by simultaneous observation of discharge pulses and vibration signal," *IEEE Transactions on Dielectrics and Electrical Insulation*, vol. 24, no. 1, pp. 288–295, Feb. 2017.

[20] Ö. Altay and Ö. Kalenderli, "Wavelet base selection for de-noising and extraction of partial discharge pulses in noisy environment," *IET Science, Measurement & Technology*, vol. 9, no. 3, pp. 276–284, May 2015.

Isara Sornsen received his B.Eng. in Electrical Engineering from North-Chiang Mai University, Chiang Mai, Thailand and M.Eng. in Electrical Engineering from Rajamangala University of Technology Lanna, Chiang Mai, Thailand. He is currently pursuing his D.Eng. in Electrical Engineering at Rajamangala University of Technology Thanyaburi, Pathum Thani, Thailand. His main research interests are partial discharge signals, and artificial intelligence.

Chatchai Suppitaksakul received his B.Eng. in Electrical Engineering from King Mongkut's Institute of Technology Ladkrabang, Bangkok, Thailand and Ph.D. in Instrumentation & Measurement, Northumbria University, Newcastle, UK. He is currently an Assistant Professor and Head of the Electrical Engineering Department, Rajamangala University of Thechnology Thanyaburi, Thailand. His research interest's digital signal and image processing, artificial intelligence, computer & machine vision and machine design.

Pollakrit Toonkum received his B.E. degree in Telecommunication Engineering from Suranaree University of Technology, Nakhon Ratchasima, Thailand, and M.Eng. and Ph.D. degrees in Electrical Engineering from the Chulalongkorn University, Bangkok, Thailand. He is currently an Assistant Professor of the Division of Mechatronics Engineering and Head of the Department of Interdisciplinary Studies, College of integrated Science and Technology, Rajamangala University of Technology Lanna, Chiang Mai, Thailand. His research interests include digital signal and image processing, artificial intelligence, and computer and machine vision.